Ionization potential of aluminum clusters

J. Akola, H. Häkkinen,* and M. Manninen
Department of Physics, University of Jyväskylä, P.O. Box 35, FIN-40351 Jyväskylä, Finland
(Received 2 February 1998)

Structure, electronic structure, and ionization potential of aluminum clusters of 2–23 atoms are studied with a total energy method based on the density-functional theory. The calculated adiabatic ionization potentials agree remarkably well with the data from threshold photoionization measurements. The analysis of results gives insight into hybridization effects in the smallest clusters as well as reveals certain clusters that exhibit a clear jellium-type shell structure. An explanation of the experimental results in the size region of 12–23 atoms is given in terms of coexisting, competing icosahedral, decahedral, and fcc-based clusters.
[S0163-1829(98)00228-8]

Measurements of the ionization potential (IP) of small metal clusters, i.e., the energy needed for removal of an electron from the cluster, yield valuable information on the electronic structure.[1] In the crudest level, the observed trends can often be understood by considering a simple model of the cluster as a conducting sphere, in which there are two contributions to the ionization potential: the binding energy of electron to the sphere (analogous to the work function W of a metal surface) and the electrostatic contribution due to the charging energy of the cluster ion. In fact, the size-evolution (apart from the well-known shell effects)[1,2] of measured ionization potentials of simple metal clusters seem to follow nicely an average trend given by $V_i(R)=W+\alpha e^2/R$, where R is the cluster radius and $\alpha=0.5$ comes from the classical charging energy of a sphere of radius R. Similarly, the electron affinity, the energy gained by attaching an electron to the cluster, is seen to follow a trend $A_e(R)=W-\beta e^2/R$, with $\alpha=\beta$ in the classical consideration. The model fulfills the obvious limit $V_i=A_e\rightarrow W$ as $R\rightarrow\infty$. With quantum corrections to the parameters α and β the measured difference V_i-A_e is reproduced reasonably well.[3]

Small aluminum clusters seem however to behave in a way that is not consistent with the above model of a metallic sphere.[4,5] There is an initial *rise* of IP up to $N=4$, i.e., $N_e=12$, N_e being the number of valence electrons. This is not explainable by the jellium model. Furthermore, strong deviations from the $\propto e^2/R$ behavior are seen up to $N\approx 20$, and even beyond. The probable explanation for the behavior of IP for small N is an incomplete s-p hybridization, whence for larger clusters there certainly are strong shell effects arising from electronic or atomic structure.[6] In this context it is interesting to note that the mass spectra in the relatively small size range (a few hundred atoms) can be explained by octahedral growth pattern, indicating that already in this size range the cluster prefers the bulk fcc symmetry.[7,8]

In this work we have studied systematically the ionization potential of small Al clusters in the size range of 2–23 atoms by an *ab initio* total energy method.[9] By analyzing the degree of s-p hybridization for the smallest clusters and the compatibility of the jellium-type shell structure for the larger ones this work is complementary to the previous semiempirical or *ab initio* calculations.[10–13] Particularly regarding the ionization potential this calculation is the most systematic one reported to date, to our knowledge. As a by-product the calculations also yield information on the geometry of the ground states of neutral and charged clusters, and some of the isomers of the neutral ones. Their effect on the measured IP will be discussed. Our results suggest an aspect that the oscillation of the measured threshold ionization in the size range of 12–23 atoms[4] is due to competition and coexistence of icosahedral, decahedral, and fcc-based structures.

The calculations are done using the BO-LSD-MD (Born-Oppenheimer local-spin-density molecular dynamics) method devised by Barnett and Landman, fully documented in Ref. 9. In the BO-LSD-MD method one solves for the Kohn-Sham (KS) one-electron equations (using a suitable parametrization for the local spin-density approximation to calculate the exchange-correlation part) for the valence electrons of the system corresponding to a given nuclear configuration of the classical ions. From the converged solution the Hellmann-Feynmann forces on ions can be calculated, which together with the classical Coulomb repulsion between the positive ion cores determine the total forces on ions, according to which one can perform structural optimizations or classical molecular dynamics for the ions. The current implementation uses plane waves combined with fast Fourier transform techniques as the basis for the one-electron wave functions and norm-conserving, nonlocal, separable[14] pseudopotentials by Troullier and Martins[15,16] to describe the valence-electron–ion interaction, and the LSD parametrization by Vosko, Wilk, and Nusair.[17] Here we wish to stress that the method does not apply any of the standard supercell techniques in calculating the total energy of a finite system. This is an important aspect pertinent to this study: the ionization potential is a straightforward difference in the total energies of the neutral and charged cluster, without or with the relaxation of the charged cluster to evaluate the vertical or adiabatic IP, respectively.

We give the ground-state structures and ionization potentials for Al–Al_7 in Table I. Table II shows IP's for Al_{12}–Al_{23}. Both tables show the experimental data by Schriver *et al.*,[4] and our adiabatic values are compared to the experimental (threshold ionization) data as well as to some earlier calculations in Fig. 1. For each cluster (both neutral and ion) we found the ground state to have the minimum total spin i.e., $S=0$ and $S=1/2$ for a cluster with even and

TABLE I. Symmetry, average bond length (in Å), experimental (Ref. 4) and calculated vertical (vIP) and adiabatic (aIP) ionization potential (in eV) for ground states of Al–Al_7.

N	Symmetry	$\langle d \rangle$	IP(exp)	vIP(LSD)	aIP(LSD)
1			5.99	6.12	
2	D_∞	2.46	6.20	6.83	6.25
3	C_{3v}	2.48	6.45	6.91	6.79
4	D_{2h}	2.58	6.55	6.80	6.69
5	C_{2v}	2.58	6.45	6.77	6.68
6	O	2.73	6.45	7.03	6.93
7	O	2.69	6.20	6.38	5.90

odd number of atoms, respectively. The only exceptions are dimer and 13-atom ion (icosahedron) with $S=1$.[18] Of the two size regimes discussed in this paper the smaller clusters are interesting due to the hybridization effects whence for the larger ones competing structural motifs were found by comparing the calculated and measured IP values.

The structures were obtained for Al_2–Al_7 by a conjugate-gradient search among a number of plausible candidates. For the size-range Al_{12}–Al_{23} we used a classical molecular dynamics program in conjunction with a potential derived from the effective medium theory (EMT) (Refs. 19 and 20) to produce a number of low-energy isomers, the best ones of which were selected as starting geometries for the BO-LSD-MD calculations. The structures were obtained by cooling from hot liquid clusters. The vast number of the lowest energy structures produced by EMT potential were icosahedral-based structures. As is well known, certain sizes

TABLE II. Ionization potentials for Al_{12}–Al_{23} (in eV). The table shows experimental values (Ref. 4) together with the calculated vIP and aIP for ICS and COS structures. Also shown is the energy difference $\Delta E = E(\text{cubo}) - E(\text{ico})$ (in K). In addition, results for decahedral structures are shown in parentheses for $N=13$ −15,22,23. In that case $\Delta E = E(\text{deca}) - E(\text{ico})$. The values in boldface are plotted in Fig. 1 for reasons explained in the text.

N	IP(exp)	vIP(LSD) ico	aIP(LSD) ico	vIP(LSD) cubo	aIP(LSD) cubo	ΔE
12	6.20	6.45	**6.30**	6.42	6.28	460
13	6.45	7.00	6.92	6.39		850
13		(6.85)	(**6.42**)			(70)
14	5.80	6.46	6.09	5.87	5.58	400
14		(6.27)	(**5.89**)			(30)
15	5.76	6.15	**5.74**	6.41	5.77	430
15		(6.21)	(5.97)			(80)
16	5.90	6.15	**6.06**	5.72	5.54	500
17	5.62	6.11	**5.63**	5.96	5.77	5
18	5.76	6.17	6.06	5.88	**5.69**	−520
19	5.56	6.20	6.14	5.82	**5.62**	60
20	5.73	6.19	6.08	5.89	**5.80**	110
21	5.56	6.23	5.99	5.84	**5.71**	2
22	5.72	6.30	5.93	5.87	5.72	460
22		(5.94)	(**5.86**)			(−90)
23	5.38	5.94	**5.76**	5.86	5.62	680
23		(6.27)	(5.95)			(−130)

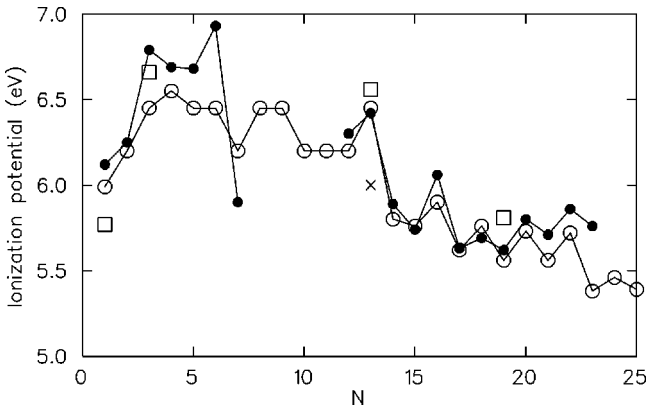

FIG. 1. Ionization potential of aluminum clusters (in eV). Open circles, threshold photoionization experiment (Ref. 4); solid dots, BO-LSD-MD results; open squares, Car-Parrinello calculations (Ref. 11); and crosses, $X\alpha$ results (Ref. 12).

(13,19,23) are particularly interesting since they match filled atomic-shell structures of either icosahedral, decahedral, or fcc-based [(cub)octahedral] symmetry (see Fig. 2). For these sizes we started optimization directly from these symmetries. All the structure optimizations were done without any constraints to the symmetry.

To analyze the hybridization of the KS states, ψ_i^{KS}, for the smallest clusters we projected each occupied state onto spherical harmonic components according to

$$\psi_i^{KS}(\mathbf{r}) = \sum_{l,m} \phi_{l,m}^i(r) Y_{l,m}(\Omega), \tag{1}$$

with l up to 3 (atomic f state), from which a weight w_l^i of a given angular momentum component in the charge density is

$$w_l^i = \sum_{m=-l}^{l} \int [\phi_{l,m}^i(r)]^2 r^2 dr. \tag{2}$$

We performed this analysis from dimer to tetramer the origin for the expansion (1) set at the atoms. We wish to note here that the plane-wave basis set prevents us from a full Mulliken analysis common in traditional quantum chemical

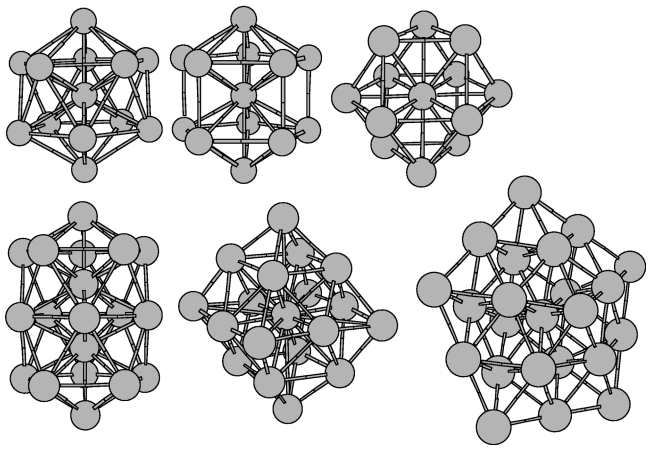

FIG. 2. Closed atomic shell structures. Top from left: 13-atom icosahedron, decahedron, and cuboctahedron. Bottom: 19-atom double icosahedron, octahedron, and 23-atom decahedron.

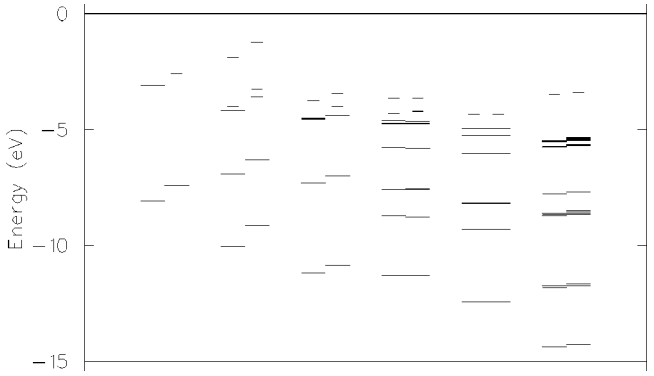

FIG. 3. Kohn-Sham one-electron eigenvalues (in eV) for selected ground-state Al_N clusters. From left: Al atom, dimer, trimer, tetramer, Al_6, and icosahedral Al_{13}. The longer and shorter lines correspond to occupied and unoccupied levels, respectively. Also the spin splitting is shown.

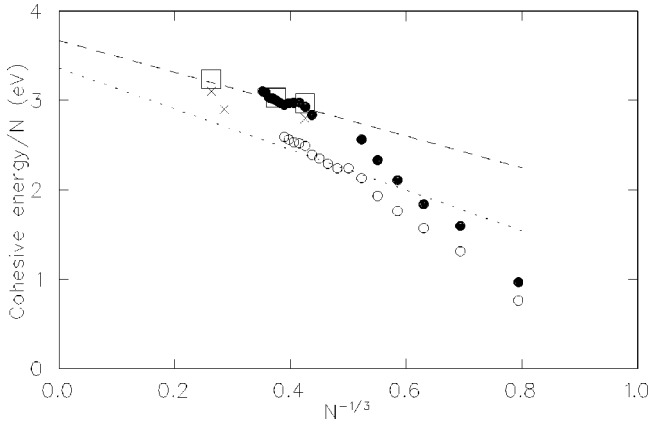

FIG. 4. Cohesive energies per atom (in eV). Open circles, photodissociation experiment (Ref. 23); solid dots, BO-LSD-MD results; open squares, Car-Parrinello calculations (Ref. 11); and crosses, $X\alpha$ results (Ref. 12). The dotted (taken from Ref. 23) and dashed lines are discussed in the text.

methods with localized basis functions on atoms. However, we have found that the average weight $\overline{w_l}$ (over all the atoms in the cluster) provides useful information on the degree of hybridization of a given KS state, which qualitatively agrees with earlier quantum chemical results.[10] According to the molecular orbital theory, four lowest and two highest states (including spin) of the dimer should derive from atomic $3s$ and $3p$ states, respectively. Indeed, we find that for the four lowest states $\overline{w_s}=0.85-0.87$ and $\overline{w_p}=0.11-0.14$, whence the two highest states are clearly p dominated with $\overline{w_p}=0.95$. For the trimer, the primary components are $\overline{w_s}=0.61-0.83$ for the six lowest states and $\overline{w_p}=0.93-0.97$ for the remaining three states. Most of the states for the tetramer are already heavily s-p mixed. As seen from Fig. 1, the calculated IP initially rises up to Al_3, leveling off after that, exhibiting a strong drop from Al_6 to Al_7. The leveling off happens around the size where s-p hybridization starts according to the above analysis.

We associate high IP's for Al_6 and Al_{13} with jellium-type shell effects. As seen from Fig. 3, Al_6 and Al_{13} show a fairly nicely grouped level structure, and having 18 and 39 electrons, respectively, are close to magic numbers of spherical jellium. We have performed angular momentum analysis also for these clusters, but now the origin for the expansion (1) was set to the center of electronic charge density of the cluster. The analysis results in the sequence $1s^2 1p^6 1d^4 (2s1d)^2 1d^4$ for occupied states for Al_6. Each angular momentum component has a weight of at least 0.94, except the mixed $(2s1d)$ state where the primary weights are $w_s=0.80$ and $w_d=0.12$. Al_{13} has a clear jellium-type sequence $1s^2 1p^6 1d^{10} 2s^2$ for the 20 lowest states. The highest occupied shell has a strong p-f mixing which is understandable since the fivefold symmetry of icosahedron is known to split $\ell=3$ orbitals. Al_6 and Al_{13} thus appear to exhibit surprisingly well-defined jellium-type shell structure. The strong drops in IP from Al_6 to Al_7 and from Al_{13} to Al_{14} thus reflect highest occupied molecular orbital states of Al_7 and Al_{14} that are above the jellium gaps at 20 and 40 electrons, respectively.

Several previous calculations have addressed the question in what size region fcc-based structures become energetically competitive with higher-symmetry structures, most notably structures based on the icosahedral symmetry. Yi *et al.* compared ideal 13-, 19-, and 55-atom cuboctahedral (COS) and icosahedral (ICS) structures by Car-Parrinello calculations[11] and found that COS gave a lower total energy for Al_{19} and Al_{55}. However, when fully annealed, Al_{55} was found to relax to a low-symmetry structure notably different from ICS or COS.[11] Cheng *et al.* performed density-functional (DFT) based discrete-variational-method $X\alpha$ calculations and found Al_{55} to prefer COS.[12] Yang *et al.*, using DFT local-orbital method, found ICS and COS to be nearly degenerate in energy for Al_{55}, but COS to have a lower energy for Al_{147}.[13]

Our calculated energy difference $E(\text{cubo})-E(\text{ico})$ for $N\geqslant 12$ is shown in Table II. In agreement with all previous calculations, we find that Al_{13} clearly prefers ICS over COS. In fact, 13-atom COS transforms to ICS in molecular dynamics runs at low temperature (<100 K).[21] In the size range of $14\leqslant N\leqslant 23$ there are certain sizes (17,19,21) where ICS slightly wins COS in energy, whence for Al_{18} COS is notably energetically favorable. The decahedron is surprisingly close to ICS for $N=13-15$, and is *the best* structure for $N=22,23$. Having in mind that in the experiment[4] (i) IP is determined from the threshold energy and (ii) the temperature of clusters is fairly low, we use the criterion that for comparison with the experiment, the *lower* calculated aIP for coexisting structures within 150 K in energy should determine the threshold energy. Otherwise, we plot in Fig. 1 the aIP of the ground state. This simple criterion produces a surprisingly good agreement with the measurement in that size range. We interpret this result as an indirect evidence that for this size region the competition between different structures becomes important.

We wish to remark here that no attempts have been made to estimate the effect of temperature on the IP.[22] Generally, finite temperature tends to lower the IP and its effect is relatively stronger in small clusters. This would further improve the agreement between our calculations and the experiment.

Finally, we show the calculated cohesive energy $E_c(N)=[E(\text{Al}_N)-NE(\text{Al})]/N$ in Fig. 4 together with some other DFT calculations[11,12] and data from photodissociation experiments by Ray *et al.*[23] Our results are generally consistent

with other DFT studies, being 0.2–0.5 eV higher than experimental values, a behavior typical to DFT with local-density approximation. The post-LSD gradient correction[9] has been calculated for some of the clusters, and its effect is to lower the LSD cohesive energy by 0.5 eV. The important feature portrayed by Fig. 4 is the fact that the experimentally determined cohesive energies even from Al_7 seem to extrapolate quite reasonably to the bulk cohesive energy (3.36 eV) just by taking a simple approximation for the per atom cluster cohesive energy $E_C(N)=\alpha-\beta N^{-1/3}$, where α is the bulk value and β accounts for surface effects (see Ref. 23). A least-square fit to our calculated values (dashed line) for $N \geqslant 12$ extrapolates to about 0.3 eV overbinding in the bulk, which is in a reasonable range with the LSD approximation.

In summary, we have studied systematically the structure, electronic structure, and ionization potential of aluminum clusters in the size range of 2–23 atoms with the BO-LSD-MD method. Our calculated adiabatic ionization potentials agree remarkably well with the data from threshold ionization measurements. The initial rise of IP as a function of cluster size is understood in terms of increasing hybridization of cluster orbitals derived from atomic s and p orbitals. Al_6 and Al_{13} have a clear shell structure in the jellium picture. We suggest that the strong oscillations in the experimental data in the region $12 \leqslant N \leqslant 23$ are due to competition and coexistence of icosahedral, decahedral, and fcc-based structures.

This work was supported by the Academy of Finland. We wish to thank Uzi Landman and Robert L. Whetten for useful discussions and to acknowledge a grant (H.H.) by the Väisälä Foundation.

*Present address: School of Physics, Georgia Institute of Technology, Atlanta, GA 30332.

[1] W. A. de Heer, Rev. Mod. Phys. **65**, 611 (1993).
[2] M. Brack, Rev. Mod. Phys. **65**, 677 (1993).
[3] M. Seidl, K.-H. Meiwes-Broer, and M. Brack, J. Chem. Phys. **95**, 1295 (1991).
[4] K. E. Schriver, J. L. Persson, E. C. Honea, and R. L. Whetten, Phys. Rev. Lett. **64**, 2539 (1990).
[5] M. F. Jarrold, J. E. Bower, and J. S. Kraus, J. Chem. Phys. **86**, 3876 (1987).
[6] T. P. Martin, Phys. Rep. **273**, 199 (1996).
[7] T. P. Martin, U. Näher, and H. Schaber, Chem. Phys. Lett. **199**, 470 (1992).
[8] S. Valkealahti, U. Näher, and M. Manninen, Phys. Rev. B **51**, 11 039 (1995).
[9] R. N. Barnett and U. Landman, Phys. Rev. B **48**, 2081 (1993).
[10] T. H. Upton, Phys. Rev. Lett. **56**, 2168 (1986); J. Chem. Phys. **86**, 7054 (1987).
[11] J.-Y. Yi, D. J. Oh, and J. Bernholc, Chem. Phys. Lett. **174**, 461 (1990); Phys. Rev. Lett. **67**, 1594 (1991).
[12] H.-P. Cheng, R. S. Berry, and R. L. Whetten, Phys. Rev. B **43**, 10 647 (1991).
[13] S. H. Yang, D. A. Drabold, J. B. Adams, and A. Sachdev, Phys. Rev. B **47**, 1567 (1993).
[14] L. Kleinman and D. M. Bylander, Phys. Rev. Lett. **48**, 1425 (1982).
[15] N. Troullier and J. L. Martins, Phys. Rev. B **43**, 1993 (1991).
[16] The pseudopotentials were generated for $3s$ (nonlocal) and $3p$ (local) electrons, with core radii $2.1a_0$ and $2.5a_0$. Using a kinetic energy cutoff $E_c^{PW}=15.4$ Ry for the plane-wave basis set the pseudoenergy and ionization potential of the atom were within 2% and 1%, respectively, of their converged values with $E_c^{PW}=89$ Ry.
[17] S. H. Vosko, L. Wilk, and M. Nusair, Can. J. Phys. **58**, 1200 (1980); S. H. Vosko and L. Wilk, J. Phys. C **15**, 2139 (1982).
[18] For the $S=1$ dimer we find two bond lengths, 2.45 Å and 2.72 Å, from which the shorter one gives slightly better (0.04 eV) bond energy, in accord with quantum chemical calculations by Upton [J. Phys. Chem. **90**, 754 (1986)], and another density-functional study (Ref. 13).
[19] K. W. Jacobsen, J. K. Nørskov, and M. J. Puska, Phys. Rev. B **35**, 7423 (1987).
[20] H. Häkkinen and M. Manninen, J. Phys.: Condens. Matter **1**, 9765 (1989).
[21] H. Häkkinen (unpublished).
[22] C. Yannouleas and U. Landman, Phys. Rev. Lett. **78**, 1424 (1997).
[23] U. Ray, M. F. Jarrold, J. E. Bower, and J. S. Kraus, J. Chem. Phys. **91**, 2912 (1989).